

Article

Photochemistry of 2-Formyl-Phenylnitrene: A Doorway to Heavy-Atom Tunneling of a Benzazirine to a Cyclic Ketenimine

Cláudio M. Nunes, Igor Reva, Sebastian Kozuch, Robert J. McMahon, and Rui Fausto

J. Am. Chem. Soc., **Just Accepted Manuscript** • DOI: 10.1021/jacs.7b10495 • Publication Date (Web): 07 Nov 2017

Downloaded from <http://pubs.acs.org> on November 7, 2017

Just Accepted

"Just Accepted" manuscripts have been peer-reviewed and accepted for publication. They are posted online prior to technical editing, formatting for publication and author proofing. The American Chemical Society provides "Just Accepted" as a free service to the research community to expedite the dissemination of scientific material as soon as possible after acceptance. "Just Accepted" manuscripts appear in full in PDF format accompanied by an HTML abstract. "Just Accepted" manuscripts have been fully peer reviewed, but should not be considered the official version of record. They are accessible to all readers and citable by the Digital Object Identifier (DOI®). "Just Accepted" is an optional service offered to authors. Therefore, the "Just Accepted" Web site may not include all articles that will be published in the journal. After a manuscript is technically edited and formatted, it will be removed from the "Just Accepted" Web site and published as an ASAP article. Note that technical editing may introduce minor changes to the manuscript text and/or graphics which could affect content, and all legal disclaimers and ethical guidelines that apply to the journal pertain. ACS cannot be held responsible for errors or consequences arising from the use of information contained in these "Just Accepted" manuscripts.

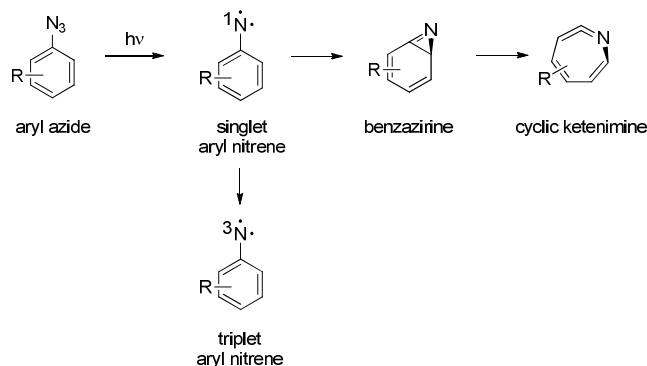


ACS Publications

INTRODUCTION

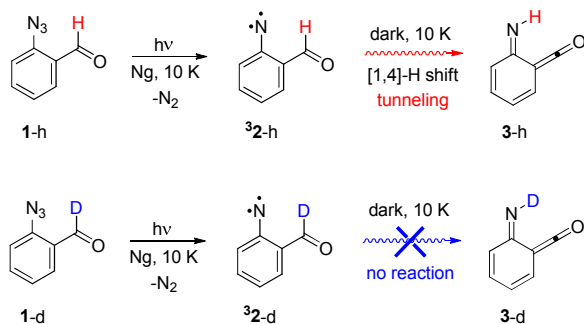
Aryl nitrenes (Ar-N) are highly reactive intermediates most commonly generated from aryl azides (Ar-N_3).¹⁻³ To shed light on the aryl azides/nitrenes chemistry and on the nature of aryl nitrene species, many studies have been carried out in last fifty years, in particular with the application of matrix isolation, time-resolved spectroscopy and quantum-mechanical computational approaches.¹⁻⁷ This knowledge has played a crucial role for the design of aryl azides that render aryl nitrenes with suitable reactivity for uses in photoresists, in photoaffinity labeling of biomolecules, and in the design of materials or organic molecules.⁸⁻¹¹

It is now well established that the photolysis of aryl azides occurs with the release of molecular nitrogen and the formation of open-shell singlet (OSS) aryl nitrene intermediates (Scheme 1). The OSS aryl nitrenes are $\sim 15 \text{ kcal mol}^{-1}$ more energetic than their triplet ground state.^{6,12,13} Therefore, upon formation of OSS aryl nitrenes, either relaxation by intersystem crossing (ISC) to triplet aryl nitrenes or competitive rearrange to benzazirines takes place, or both, depending on the experimental conditions and on the characteristics of the aryl substituents. With a few exceptions, the formation of benzazirines is the rate-limiting step of the process of aryl nitrene isomerization to cyclic ketenimines. The barrier of ring expansion from benzazirines to cyclic ketenimines is quite small ($\sim 3 \text{ kcal mol}^{-1}$ computed for parent species),^{6,14} which makes very challenging and rare the capture and direct observation of benzazirines.¹⁵⁻¹⁸



Scheme 1. General mechanism for the photochemistry of aryl azides.

The slippery potential energy surface of aryl nitrenes hides, however, other fascinating reactions. Some of us have recently found the first indication of heavy-atom tunneling for the ring expansion of a benzazirine to a cyclic ketenimine.¹⁵ It was observed that methylthio-substituted benzazirine, generated in the photochemistry of 4-methylthio-phenylazide, spontaneously rearranges in cryogenic matrices to the corresponding cyclic ketenimine. In contrast, under similar conditions, methoxy-substituted benzazirine, generated in the photochemistry of 4-methoxy-phenylazide, was found to be stable. Furthermore, we have also recently revealed the first direct evidence of a tunneling reaction in the aryl nitrene chemistry.¹⁹ It was found that triplet 2-formyl-phenylnitrene **3**²-h, generated from 2-formyl-phenylazide **1**-h, spontaneously rearranges into imino-ketene **3**-h in the dark at 10 K (Scheme 2). Under the same conditions, the deuterium derivative **3**²-d was observed to be stable, strongly supporting the occurrence of a tunneling mechanism as opposed to a thermally activated process.



Scheme 2. Tunneling reaction of triplet 2-formyl-phenylnitrene **3**²-h to imino-ketene **3**-h directly observed in (Ng = noble gas) cryogenic matrices.¹⁹

Quantum mechanical tunneling is an intriguing phenomenon that is becoming recognized as crucial to understand the reactivity of some organic reactions and even some biological processes that involve displacement of a light hydrogen atom.^{20–23} Because the quantum tunneling probability decreases exponentially with the square root of the shifting mass, the observation of heavy-atom tunneling (involving the displacement of non-hydrogen atoms) is very rare.²⁴ There are six reactions known where experimental evidence was obtained for heavy-atom tunneling occurring under cryogenic conditions

1 from the ground vibrational state:²⁵ the automerization of cyclobutadiene,²⁶ the ring expansion reactions
2 of methylcyclobutylfluorocarbene,²⁷ noradamantylchlorocarbene,²⁸ strained cyclopropane
3
4 1*H*-bicyclo[3.1.0]-hexa-3,5-dien-2-one²⁹ and methylthio substituted benzazirine,¹⁵ and the Cope
5
6 rearrangement of dimethylsemibullvalene³⁰. Nonetheless, computational chemists have been
7
8 discovering and predicting that carbon atom tunneling would contribute to many more reactions.^{24,31}
9

10
11 Herein, we report new results obtained in the quest for elusive reactions on potential energy surface of
12
13 aryl nitrenes. Using low-temperature matrix isolation coupled with IR spectroscopy and a tunable
14
15 narrowband radiation source, the photochemistry of protium ³**2**-h and deuterated ³**2**-d triplet 2-formyl-
16
17 phenylnitrene was investigated and one interesting case of heavy-atom tunneling consisting in the ring
18
19 expansion reaction of the corresponding benzazirine to cyclic ketenimine was discovered. Computations
20
21 performed using small curvature tunneling approximation and canonical variational transition state
22
23 theory confirm that the reaction can only occur by a tunneling process from the ground state at
24
25 cryogenic conditions.
26
27
28
29
30
31
32
33
34
35
36
37
38
39
40
41
42
43
44
45
46
47
48
49
50
51
52
53
54
55
56
57
58
59
60

RESULTS AND DISCUSSION

Photochemistry of 2-formyl-phenylnitrene

Few minutes irradiation at $\lambda = 308$ nm of deuterated 2-formyl-phenylazide **1-d**, isolated in an argon matrix at 10 K, gives mainly triplet deuterated 2-formyl-phenylnitrene **³2-d**.³² As shown in Figure 1, the experimental IR bands of the photoproduct are in excellent agreement with the IR spectrum of **³2-d** calculated at the B3LYP/6-311++G(d,p) level. The comprehensive assignment of the experimental IR spectrum of triplet deuterated 2-formyl-phenylnitrene **³2-d** is given in Table S1. The irradiation, under similar conditions, of protium 2-formyl-phenylazide **1-h** produces mainly triplet 2-formyl-phenylnitrene **³2-h**, which spontaneously rearranges by tunneling to imino-ketene **3-h**.¹⁹ In contrast to the behavior of nitrene **³2-h**, deuterated nitrene **³2-d** is stable against tunneling in argon matrix at 10 K.

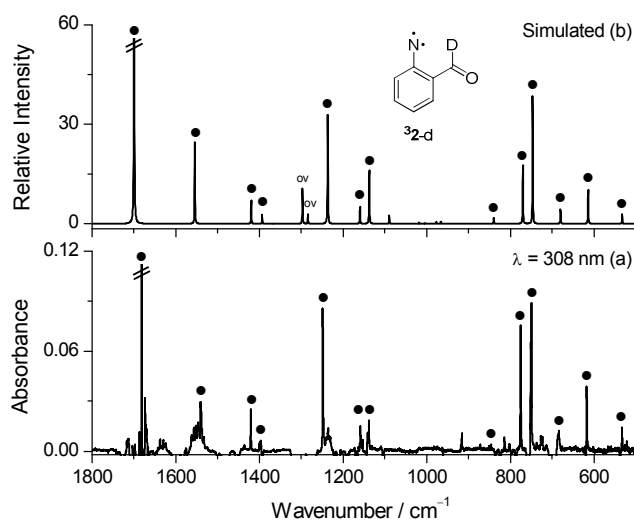


Figure 1. (a) Experimental difference IR spectrum obtained as the spectrum after UV irradiation at $\lambda = 308$ nm (240 s, 3 mW) of deuterated 2-formyl-phenylazide **1-d** isolated in an argon matrix at 10 K “minus” the spectrum of **1-d** before irradiation. The negative bands (truncated) are due to the consumed **1-d** (at this stage ~60 %). The positive bands labeled with black circles (●) are assigned to triplet deuterated 2-formyl-phenylnitrene **³2-d**. (b) IR spectrum of **³2-d** simulated at B3LYP/6-311++G(d,p) level. The labels “ov” indicate IR bands of **³2-d** overlapped with more intense bands due to the **1-d** precursor.

Subsequently, the photochemistry of **³2-d** was investigated by performing irradiations using longer wavelengths, where the remained precursor **1-d** does not absorb. Starting with irradiations at $\lambda = 600$ nm

and gradually decreasing the wavelength, it was found that nitrene **32-d** starts to react at around $\lambda = 530$ nm.³³ Figure 2 shows the results of irradiation at $\lambda = 530$ nm during a total time of 40 min, when the consumption of **32-d** is ~ 70 %. Concomitantly with consumption of **32-d**, at least three different photoproducts labeled as **A** (2112 cm^{-1}), **B** (1839 cm^{-1}) and **C** ($1695/1688\text{ cm}^{-1}$) were identified. The amount of photoproduct **A** was found to reach its maximum at the current stage of irradiation ($t = 40$ min). The continuation of irradiation ($\lambda = 530$ nm) led to a decrease in the total amount of **A** and a significant increase in the total amount of **B** (Figure S1). This kinetic trend strongly suggests that **B** is not directly formed from the nitrene **32-d**.

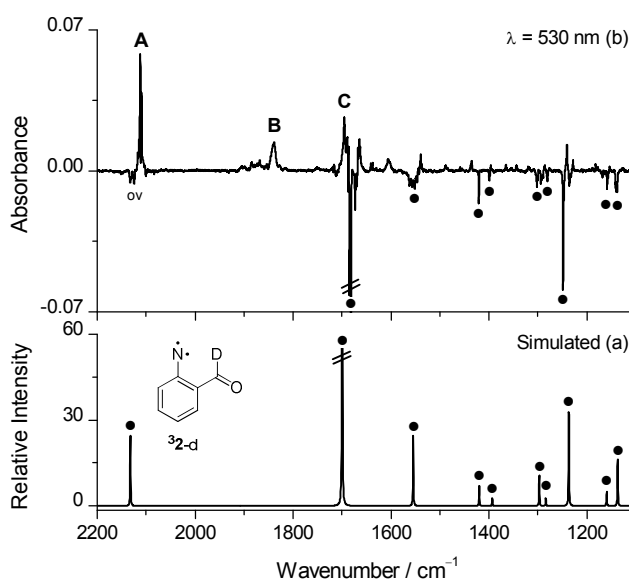


Figure 2. (a) IR spectrum of triplet deuterated 2-formyl-phenylnitrene **32-d** simulated at B3LYP/6-311++G(d,p) level. (b) Experimental difference IR spectrum showing changes after irradiation at $\lambda = 530$ nm (40 min, 90 mW), subsequent to irradiation at $\lambda = 308$ nm (see Figure 1). The negative bands are due to the consumed nitrene **32-d** (at this stage ~ 70 %). The positive bands labeled **A**, **B** and **C** are the most characteristic bands of the identified photoproducts. The label “ov” indicates an IR band of **32-d** overlapped with a more intense band due to the photoproduct **A**.

Indeed, after the irradiation at $\lambda = 530$ nm during a total time of 160 min (when almost all nitrene **32-d** is consumed; Figure S1), it was found that subsequent irradiations at $\lambda = 500$ nm convert **A** into **B** (Figure 3b).³⁴ The experimental IR signature of the consumed **A** compares very well with the IR

spectrum of N-deuterated imino-ketene **3-d** calculated at B3LYP/6-311++G(d,p) level (Figure 3a-b). The most intense band observed in the IR spectrum of **A** appears at 2112 cm^{-1} , a frequency region where ketenes usually have characteristic strong $\nu(\text{C}=\text{C}=\text{O})_{\text{as}}$ absorption (e.g. typically around 2100 cm^{-1}).³⁵ Actually, this band compares well with the $\nu(\text{C}=\text{C}=\text{O})_{\text{as}}$ band described at 2110 cm^{-1} for the protium imino-ketene **3-h** analogue, which is formed by 2-formyl-phenylnitrene **3-h** tunneling.¹⁹ Other characteristic IR bands of **A** are observed at 1637, 1547, 1540 and $621/616\text{ cm}^{-1}$, in good correspondence with the IR bands of **3-d** calculated at 1645 [$\nu(\text{C}=\text{C})_{\text{as}}$], 1555 [$\nu(\text{C}=\text{N})$], 1541 [$\nu(\text{C}=\text{C})_{\text{s}}$] and $607\text{ }[\tau(\text{N}-\text{D})]\text{ cm}^{-1}$. A more comprehensive assignment of the observed IR spectrum of product **A**, identified as N-deuterated imino-ketene **3-d**, is given in Table S2.

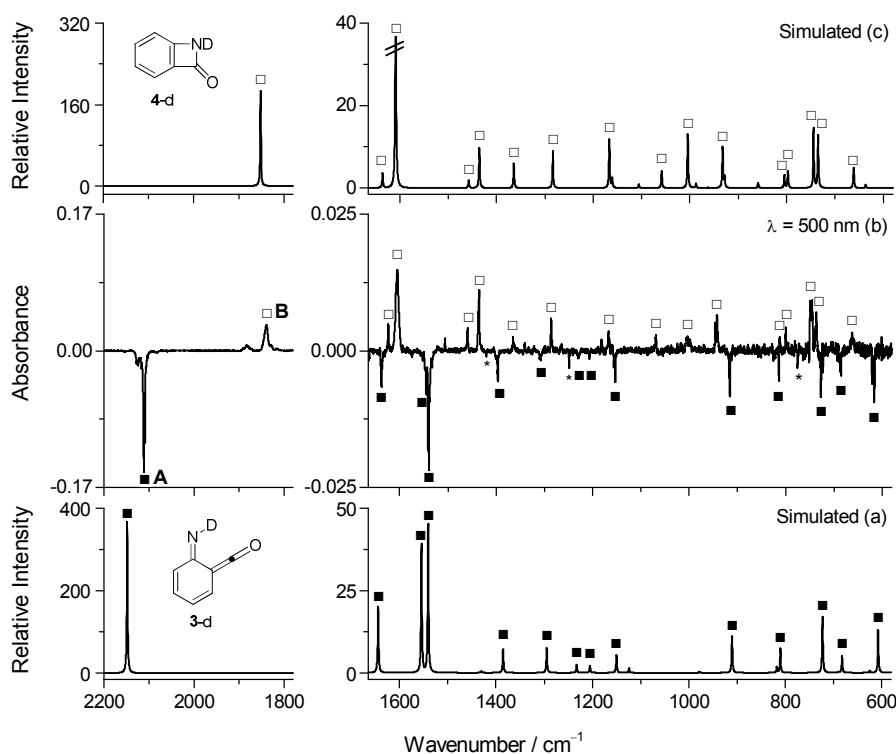


Figure 3. (a) IR spectrum of N-deuterated imino-ketene **3-d** simulated at B3LYP/6-311++G(d,p) level. (b) Experimental difference IR spectrum showing changes after irradiation at $\lambda = 500\text{ nm}$ (100 min, 60 mW), subsequent to irradiation at $\lambda = 530\text{ nm}$ that consumed nitrene **3-d** (Figure S1). The negative bands are due to the consumed **A** assigned to imino-ketene **3-d** (solid squares, ■). The positive bands are due to the formation of **B** assigned to benzoazetinone **4-d** (empty squares, □). Asterisks (*) indicate the bands due to traces of nitrene **3-d** consumed. (c) IR spectrum of N-deuterated benzoazetinone **4-d** simulated at B3LYP/6-311++G(d,p) level.

The experimental IR signature of the photoproduct **B** was found to compare very well with the IR spectrum of N-deuterated benzoazetinone **4-d** calculated at B3LYP/6-311++G(d,p) level (Figure 3b-c). The most intense band observed in the IR spectrum of **B** at 1836 cm⁻¹ correlates well with the most intense band predicted in the IR spectrum of **4-d** at 1852 [$\nu(\text{C}=\text{O})$] cm⁻¹. This assignment is also supported by the frequency proximity between the band at 1836 cm⁻¹ and the strong carbonyl stretching at 1843 cm⁻¹ described for the N-methyl benzoazetinone analogue,³⁶ which are typical of the $\nu(\text{C}=\text{O})$ frequencies where the carbonyl group is inserted in a 4-membered ring.³⁷ Other characteristic IR bands of **B** are observed at 2543/2533 and 1605 cm⁻¹, fitting well with the IR bands of **4-d** calculated at 2535 [$\nu(\text{N}-\text{D})$] and 1608 [ring stretching] cm⁻¹. A more complete assignment (total of 19 bands) of the observed IR spectrum of **B**, identified as N-deuterated benzoazetinone **4-d**, is given in Table S3.

The photochemical transformation of an imino-ketene into a benzoazetinone is not unprecedented. Dunkin et al.³⁶ and Tomioka et al.³⁸ reported that analogous N-methyl and N-methoxy imino-ketenes undergo ring closure to the corresponding N-substituted benzoazetines in argon matrix, upon irradiation with $\lambda > 400$ nm. The identification of those imino-ketenes and benzoazetines was performed mainly by their characteristic $\nu(\text{C}=\text{C}=\text{O})_{\text{as}}$ and $\nu(\text{C}=\text{O})$ bands, respectively (Scheme S2). In the current work, the transformation of imino-ketene **3-d** into benzoazetinone **4-d** was established much more comprehensively, based on the experimental identification of the almost complete mid-IR spectra of these species.

Ring expansion of benzazirine into cyclic ketenimine

Interestingly, besides the photochemical conversion of **3-d** (**A**) into **4-d** (**B**), we found that **C** spontaneously rearranges into a new product labeled as **D** (1890/1880 cm⁻¹). To observe this transformation in detail, a new experiment was performed where first the nitrene **3-d** was transformed by irradiation at $\lambda = 530$ nm and then the sample was kept at 10 K in the spectrometer beam for 3 days. After that time, the rearrangement of **C** into **D** was practically completed and the change in the experimental IR spectrum were analyzed (Figure 4b). The IR spectrum of the consumed **C** is readily

assigned to deuterated formyl benzazirine **5-d** based on the good agreement between the experimental and the calculated IR spectra (Figure 4a,b). The cyclization of nitrene **2-d** may proceed “towards” and “away” from the formyl substituent giving two isomeric benzazirines; each having two possible conformers regarding orientation of the formyl group (Table S4). Vibrational calculations on these four structures revealed that only **5-d** (the most stable form) is compatible with the experimental IR spectrum of **C** (Figure S2 and S3). The most characteristic IR bands of **C** are observed at ~ 2100 , 1751 , ~ 1700 and 1241 cm^{-1} in good agreement with the estimated IR bands of **5-d** at $2109\text{ [}\nu(\text{OC-D})\text{]}$, $1802\text{ [}\nu(\text{C=N})\text{]}$, $1710\text{ [}\nu(\text{C=O})\text{]}$ and $1221\text{ [}\nu(\text{ODC-C})\text{] cm}^{-1}$. A slight overestimation of the B3LYP calculated $\nu(\text{C=N})$ frequency of **5-d** ($\sim 50\text{ cm}^{-1}$) is consistent with the overestimation trend observed for other benzazirines¹⁶ (see also data presented in Table S5). A more detailed assignment of the IR spectrum of **C**, identified as benzazirine **5-d**, is given in Table 1.

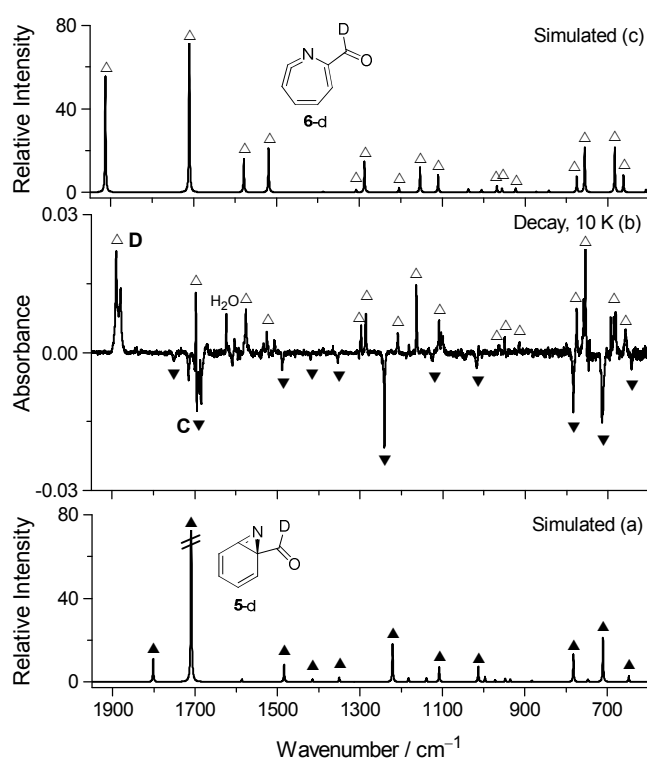


Figure 4. (a) IR spectrum of deuterated formyl benzazirine **5-d** simulated at B3LYP/6-311++G(d,p) level. (b) Experimental difference IR spectrum showing changes occurred after keeping the sample at 10 K in the spectrometer beam for ~ 3 days, subsequent to irradiation at $\lambda = 530\text{ nm}$ that consumed almost all triplet nitrene **2-d**. The negative bands are due to the consumed **C** assigned to benzazirine **5-d** (solid triangles, ▲). The positive bands are due to the formation of **D** assigned to cyclic ketenimine **6-d** (empty triangles, △). (c) IR spectrum of deuterated formyl cyclic ketenimine **6-d** simulated at B3LYP/6-311++G(d,p) level.

Table 1. Experimental IR spectral data (argon matrix at 10 K), B3LYP/6-311++G(d,p) calculated vibrational frequencies (ν , cm^{-1}), absolute infrared intensities (A^{th} , km mol^{-1}), and vibrational assignment of deuterated formyl benzazirine **5-d**.^a

Ar matrix ^b		Calculated ^c		Approx. assignment ^d
ν	I	ν	A^{th}	
2108/2097/2093	ov/br/m	2109	59.8	$\nu(\text{C-D})$
1751	w	1802	34.8	$\nu(\text{C=N})$
1706/1695/1689/1685	ov/s/s/s	1710	341.3	$\nu(\text{C=O})$
1595/1589	ww/vw	1586	3.7	$\nu(\text{C=C})_{\text{as}}$
1488	m	1484	26.3	$\nu(\text{C=C})_{\text{s}}$
1419	vw	1415	3.9	$\delta 1(\text{C-H})$
1355	w	1351	7.0	$\delta 2(\text{C-H})$
1241	s	1221	57.4	$\nu(\text{C2-C1})$
1189	vw	1183	5.5	$\delta 3(\text{C-H})$
1143	vw	1139	6.0	$\delta 4(\text{C-H})$
1125	br	1108	22.5	$\nu(\text{C3-C2-C1})_{\text{as}}, \delta(\text{C-D})$
1018/1016	br	1013	23.3	$\delta 1(6\text{-ring})$
1004	vw	997	7.8	$\delta(\text{C-D})$
947	vw/ov	948	5.0	$\gamma 1(\text{C-H}) + \nu(\text{C6-C5})$
-	-	936	4.4	$\gamma 1(\text{C-H}) - \nu(\text{C6-C5})$
784/782	s/s	783	41.2	$\gamma 2(\text{C-H})$
747	w/ov	747	4.3	$\delta 2(6\text{-ring})$
714/712	s/s	711	67.4	$\gamma 3(\text{C-H})$
643/640	m/w	649	8.5	$\tau 1(6\text{-ring})$

^aDeuterated formyl benzazirine **5-d** was generated by irradiation of deuterated 2-formyl-phenylnitrene **3-d** in an argon matrix at 10 K. Only bands in the 2600–600 cm^{-1} region having calculated intensities above 3 km mol^{-1} are included. ^bExperimental intensities are presented in qualitative terms: s = strong, m = medium, w = weak, vw = very weak, br = broad, and ov = overlapped. ^cB3LYP/6-311++G(d,p) calculated scaled frequencies. ^dAssignments made by inspection of Chemcraft animations. Abbreviations: ν = stretching, δ = bending, γ = rocking, τ = torsion, s = symmetric, as = antisymmetric, and 6-ring = six-membered ring. Signs “+” and “-” designate combinations of vibrations occurring in “syn”-phase (“+”) and in “anti”-phase (“-”). ^eFor atom numbering see Scheme S1.

The IR spectrum of the produced **D** is assigned to deuterated formyl cyclic ketenimine **6-d** based on the good match between the experimental and calculated IR spectra (Figure 4b,c). Cyclic ketenimines are known to have a characteristic strong IR absorption near 1900 cm^{-1} , due to $\nu(\text{C=C=N})_{\text{as}}$ vibration,^{16,39–41} which correlates well with the most intense band observed in the IR spectrum of **D** at 1890/1880 cm^{-1} . Other characteristic bands of **D** are observed at 2137/2117, 1698, 1576 and ~1525 cm^{-1} in good agreement with the estimated IR bands of **6-d** at 2109 [$\nu(\text{OC-D})$], 1711 [$\nu(\text{C=O})$], 1579 [$\nu(\text{C=C})_{\text{as}}$] and 1519 [$\nu(\text{C=C})_{\text{s}}$] cm^{-1} . Four different cyclic ketenimine structures may, in principle, be formed in the chemistry of nitrene **2-d** (Table S6). Based on vibrational calculations, only the **6-d** form

matches the experimental IR spectrum of **D** (Figure S4 and S5). The formation of this structure is in accordance with the expectations because the ring expansion via C–C cleavage in benzazirine isomer **5-d** directly results in cyclic ketenimine isomer **6-d**.⁴² A detailed assignment of the IR spectrum of **D**, identified as cyclic ketenimine **6-d**, is given in Table 2.

Table 2. Experimental IR spectral data (argon matrix at 10 K), B3LYP/6-311++G(d,p) calculated vibrational frequencies (ν , cm^{-1}), absolute infrared intensities (A^{th} , km mol^{-1}), and vibrational assignment of deuterated formyl cyclic ketenimine **6-d**.^a

Ar matrix ^b		Calculated ^c		Approx. assignment ^d
ν	I	ν	A^{th}	
2133/2117	vw/ov	2128	65.6	$\nu(\text{C-D})$
1890/1880	s/s	1913	175.0	$\nu(\text{C=C=N})_{\text{as}}$
1698	s/ov	1711	236.7	$\nu(\text{C=O})$
1576	m	1579	50.5	$\nu(\text{C=C})_{\text{as}}$
1533/1525	vw/w	1519	66.5	$\nu(\text{C=C})_{\text{s}}$
1297	w	1308	3.9	$\delta 1(\text{C-H})$
1286	m	1288	46.3	$\delta 2(\text{C-H})$
1208	w	1205	6.7	$\delta 3(\text{C-H})$
1164	m	1154	38.0	$\nu(\text{C2-C1})$
1110/1004	w	1110	26.2	$\delta 4(\text{C-H})$
-	-	1037	4.9	$\nu(\text{C7C6}) - \nu(\text{C5C4})$
-	-	1005	3.7	$\delta(\text{C-D})$
965/962	vw/vw	968	9.4	$\nu(\text{C7C6}) + \nu(\text{C5C4})$
950/949	w/w	956	5.8	$\gamma 1(\text{C-H})$
916/914	vw/vw	923	5.5	$\delta 1(\text{ring})$
-	-	843	3.1	$\gamma(\text{C-D}), \delta 2(\text{ring})$
776	m	775	24.2	$\gamma 2(\text{C-H})$
759/756/755	m/m/s	756	68.1	$\gamma 3(\text{C-H})$
686/681	m/m	684	67.7	$\gamma 4(\text{C-H})$
658	w	663	25.9	$\delta(\text{C=C=N})$
602	vw	609	3.9	$\tau 1(\text{ring})$

^aDeuterated formyl cyclic ketenimine **6-d** was generated by ring expansion of deuterated formyl benzazirine **5-d** in an argon matrix at 10 K. Only bands in the 2600–600 cm^{-1} region having calculated intensities above 3 km mol^{-1} are included.

^bExperimental intensities are presented in qualitative terms: s = strong, m = medium, w = weak, vw = very weak, and ov = overlapped. ^cB3LYP/6-311++G(d,p) calculated scaled frequencies. ^dAssignments made by inspection of Chemcraft animations. Abbreviations: ν = stretching, δ = bending, γ = rocking, τ = torsion, s = symmetric, and as = antisymmetric. Signs “+” and “–” designate combinations of vibrations occurring in “syn”-phase (“+”) and in “anti”-phase (“–”). ^eFor atom numbering see Scheme S1.

A similar approach was applied to investigate the possibility of ring expansion in the protium benzazirine **5-h**. Triplet 2-formyl-phenylnitrene **3-h** was first produced by irradiation of 2-formyl-phenylazide **1-h** and then immediately exposed to irradiation at $\lambda = 530$ nm. The photochemistry of **3-h**

is similar to that described for $^3\mathbf{2}\text{-h}$; at least three different products labeled as \mathbf{A}' (2111 cm^{-1}), \mathbf{B}' (1843 cm^{-1}) and \mathbf{C}' ($\sim 1710\text{ cm}^{-1}$) were formed (Figure S6 and S7). However, it must be noted that tunneling reaction of $^3\mathbf{2}\text{-h}$ to imino-ketene $\mathbf{3}\text{-h}$ ($\tau_{1/2} \sim 6\text{ hours}$)¹⁹ occurs simultaneously with the photochemistry triggered at $\lambda = 530\text{ nm}$. After 1 hour of irradiation at this wavelength only a few percent of $^3\mathbf{2}\text{-h}$ ($<10\%$) remained. The nitrene $^3\mathbf{2}\text{-h}$ is difficult to convert in its totality through irradiation at 530 nm on during this time scale because the formation of $\mathbf{3}\text{-h}$ (\mathbf{A}') that also absorbs at $\lambda = 530\text{ nm}$ and is transformed into benzoazetinone $\mathbf{4}\text{-h}$ (\mathbf{B}'). Thus, after the irradiation at $\lambda = 530\text{ nm}$, the remaining nitrene $^3\mathbf{2}\text{-h}$ was first allowed to disappear in the dark by tunneling and subsequently the sample was kept at 10 K in the spectrometer beam for 3 days. At that time, the rearrangement of \mathbf{C}' into \mathbf{D}' was completed and the IR difference spectrum corresponding to this transformation was obtained (Figure 5b).

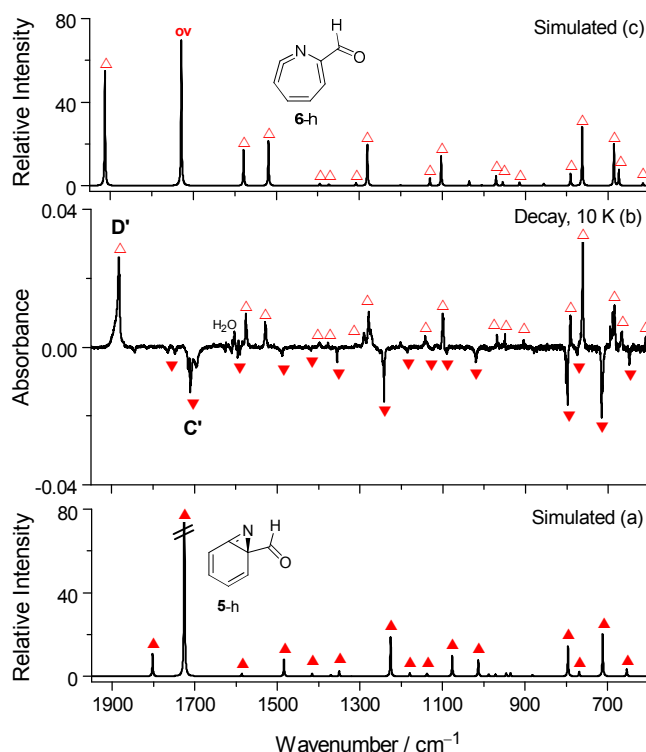


Figure 5. (a) IR spectrum of formyl benzazirine **5-h** simulated at B3LYP/6-311++G(d,p) level. (b) Experimental difference IR spectrum showing changes occurred after keeping the sample at 10 K in the spectrometer beam for 3 days, subsequent to irradiation at $\lambda = 530\text{ nm}$ and after the decay of the remained triplet nitrene $^3\mathbf{2}\text{-h}$. The negative bands are due to the consumed \mathbf{C}' assigned to benzazirine **5-h** (solid triangles, \blacktriangle). The positive bands are due to the formation \mathbf{D}' assigned to cyclic ketenimine **6-h** (empty triangles, \triangle). (c) IR spectrum of formyl cyclic ketenimine **6-h** simulated at B3LYP/6-311++G(d,p) level.

Based on the excellent agreement between the experimental and calculated IR spectra, the consumed species **C'** was assigned to formyl benzazirine **5-h** and the produced species **D'** assigned to formyl cyclic ketenimine **6-h** (Figure 5, Tables S7 and S8). Hence, in addition to the experiment described above for the deuterated derivative, we also found that protium benzazirine **5-h** undergoes ring expansion to cyclic ketenimine **6-h**.

Kinetics of the benzazirine ring expansion to cyclic ketenimine

To better understand the nature of the transformation of benzazirine into cyclic ketenimine, their respective decrease and increase were followed by IR spectroscopy (using the bands at 1241 cm^{-1} for **5-d** and 1890 cm^{-1} for **6-d** for the deuterated derivative, and using the bands at 1242 cm^{-1} for **5-h** and 1883 cm^{-1} for **6-h** for the protium derivative) while keeping the sample under different given sets of conditions. For “unfiltered IR light” conditions, the kinetics of rearrangement of benzazirine **5-d** into cyclic ketenimine **6-d** was measured when the sample was kept at 10 K and permanently exposed to the IR light source of the FTIR spectrometer. As shown in Figure 6, the data are nicely fitted by equations of mono-exponential decay kinetics, with a rate constant of $\sim 1.5 \times 10^{-5}\text{ s}^{-1}$ and a half-life of ~ 13 hours. For “dark” conditions, new experiments were performed where the sample was kept at 10 K in dark with only exception when monitoring the IR spectra, which was performed using a cutoff filter transmitting only below 2200 cm^{-1} placed between the sample and the spectrometer IR light source. As shown in Figure 7, under “dark” conditions (Kinetics 1) only $\sim 25\%$ of **5-d** rearranged to **6-d** upon 5 days. After this period of 5 days, “unfiltered IR light” conditions were applied (Kinetics 2) to confirm that a much faster rate of the rearrangement occurs under the influence of IR light. The “dark” kinetics (Figure 7, Kinetics 1) shows some dispersive character, i.e. it deviates from the first-order kinetics and exhibits a distribution of rate constants that decrease over time. This is commonly observed for reactions in cryogenic matrices and is generally attributed to distributions of matrix sites and weak interactions between substrate and the matrix environment.^{15,19,27–30} Anyway, for the sake of a rough estimate, the data for “dark” kinetics were fitted by using classical equations of mono-exponential decay, resulting in a rate constant of $\sim 7.4 \times 10^{-7}\text{ s}^{-1}$ and a half-life of ~ 260 hours. This “dark” rate constant is more than an order of magnitude smaller than the “unfiltered light” rate constant, unmistakably indicating a significant difference in both kinetics.

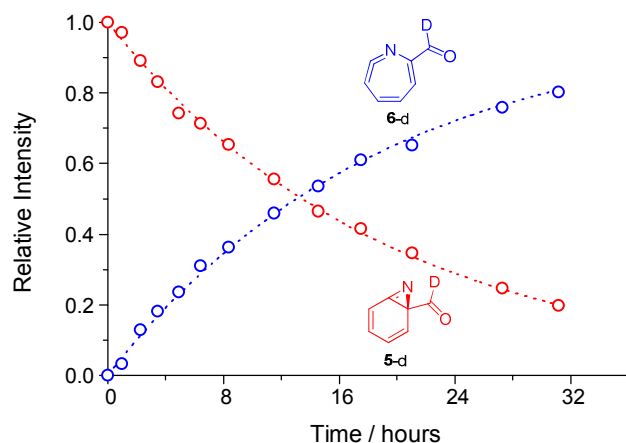


Figure 6. Kinetics of rearrangement of benzazirine **5-d** to cyclic ketenimine **6-d** in an argon matrix at 10 K, with the sample exposed to the IR light source of the FTIR spectrometer. Empty red (○) and blue (○) circles represent the time evolution of the amounts of **5-d** (consumption, measured using the peak at 1241 cm^{-1}) and **6-d** (production, measured using the peak at 1890 cm^{-1}), respectively. Red and blue dotted lines represent best fits obtained using first-order exponential kinetics equations. The rate constants are $k_{5-d} = 1.4 \times 10^{-5}\text{ s}^{-1}$ and $k_{6-d} = 1.5 \times 10^{-5}\text{ s}^{-1}$. More details are given in the experimental section.

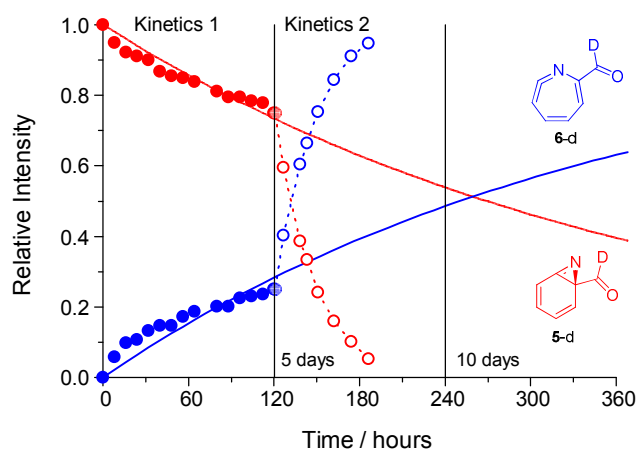


Figure 7. Kinetics of rearrangement of benzazirine **5-d** (measured using the peak at 1241 cm^{-1}) to cyclic ketenimine **6-d** (measured using the peak at 1890 cm^{-1}) in an argon matrix at 10 K. Kinetics 1 (initial 5 days, left): rearrangement of **5-d** (solid red circles (●), consumption) into **6-d** (solid blue circles (●), production) with the sample kept in dark, except when the spectra were recorded, the sample was then protected by an infrared longpass cutoff filter transmitting only below 2200 cm^{-1} . Kinetics 2 (after 5 days in dark, right): rearrangement of **5-d** (empty red circles (○), consumption) into **6-d** (empty blue circles (○), production) with the sample permanently exposed to the IR light source of the FTIR spectrometer. Blue and red solid lines represent best fits obtained using first-order single exponential kinetics equations, and adjustments were made using only the amounts of the reactant **5-d** and the product **6-d** during the first 5 days of observation (sample in dark), corresponding to $\sim 25\%$ of the conversion. The rate constants are $k_{5-d} = 7.1 \times 10^{-7}\text{ s}^{-1}$ and $k_{6-d} = 7.7 \times 10^{-7}\text{ s}^{-1}$. Blue and red dotted lines (right) are presented to guide the eye only.

1 In other independent experiment, “filtered IR light” conditions were applied, whereas a cutoff filter
2 transmitting light only below 2200 cm^{-1} was placed between the IR light source of the FTIR
3 spectrometer and the sample. In that case, the sample was exposed to filtered light continuously (i.e.,
4 including periods between the registrations of spectra). The obtained kinetics for “filtered light” decay
5 was found to be similar to the “dark” decay kinetics.
6
7
8
9
10
11
12

13 Experiments were also carried out to measure the kinetics of rearrangement of protium benzazirine
14 **5-h** into protium cyclic ketenimine **6-h**. As shown in Figure S8, under “dark” conditions (Kinetics 1) the
15 rearrangement after 5 days amounts to $\sim 27\%$. Afterwards, “unfiltered IR light” conditions were applied
16 (Kinetics 2) and a strong increase in the reaction rate was observed, similarly to the behavior found for
17 the deuterated derivative. Again, similarly to the deuterated compound, the kinetics of rearrangement
18 from **5-h** to **6-h** in the dark has some dispersive character. To obtain a rough estimate, the data for
19 “dark” kinetics were fitted by using equations of the first-order kinetics, resulting in a rate constant of
20 $\sim 8.8 \times 10^{-7}\text{ s}^{-1}$ and a half-life of ~ 219 hours. This rate constant of the rearrangement from **5** to **6** under
21 “dark” conditions of protium compound differs somewhat from the analogous rate found for the
22 deuterated analogue. Even within the measurement accuracy of peak intensities of the bands used and
23 also with the caveat that a single-exponential fitting is, only approximately applicable to trace the
24 dispersive kinetics, these rates suggest a small decrease in the rate resulting from the substitution of
25 protium with deuterium in the carbonyl group of **5**. Indeed, as it will show in the next section,
26 computations indicate that the secondary kinetic isotope effect is significant.
27
28
29
30
31
32
33
34
35
36
37
38
39
40
41
42
43
44
45

46 To verify if the rearrangement is not activated thermally, we carried out additional kinetic
47 measurements of the rearrangement of **5-d** to **6-d** at 20 K also under dark conditions (Figure S9). Again,
48 even though the kinetics has some dispersive character, the data were adjusted by using the first-order
49 kinetic equations and a rough rate constant was estimated as $\sim 8.9 \times 10^{-7}\text{ s}^{-1}$ and a half-life of ~ 216
50 hours. Within the precision of estimations and considering the data from a semi-qualitative perspective,
51 the rate of the rearrangement hardly shows any increase upon increase of the absolute temperature by a
52
53
54
55
56
57
58
59
60

factor of two. The matrix softening induced by the temperature increase can be responsible for the possible small acceleration of the rearrangement, as proposed for other cases of tunneling reactions in matrices.^{15,27–30}

CCSD(T) computations (see below) estimate an energy barrier of 7.5 kcal mol⁻¹ for the rearrangement of **5** to **6** (~1.4 kcal mol⁻¹ more stable). This energy barrier is far too high to afford a thermal activation at the low working temperatures up to 20 K under “dark” conditions. Moreover, attaining such a high barrier seems not possible under the experimental “filtered light” condition, when the sample at 10 K is exposed to light with wavenumbers below 2200 cm⁻¹ (~6.3 kcal mol⁻¹ or less). The data indicate therefore that the rearrangement of benzazirine **5** to cyclic ketenimine **6** in low temperature matrix occurs through heavy-atom tunneling. Because the reaction rate under “dark” conditions is similar to the rate when the sample is exposed to “filtered IR light” conditions, the vibrationally assisted tunneling is unlikely.

In the case of “unfiltered light” conditions, the observed significantly faster rate, compared to “dark” or “filtered IR light” conditions, suggests the occurrence of IR-induced photochemistry. Here the sample is clearly exposed to light with energy well above the calculated barrier.⁴³ The energy deposited in vibrational modes of benzazirine **5** located above the reaction barrier, for instance into the CH stretching modes or in any overtone/combination transition with frequency above ~2625 cm⁻¹ (7.5 kcal mol⁻¹) may promote isomerization to cyclic ketenimine **6** (Figure S10). In the opposite direction, from **6** to **5**, the estimated reaction barrier is higher, ca. ~8.9 kcal mol⁻¹ (~3125 cm⁻¹). This barrier is above the energy of the CH stretching modes (~3000 cm⁻¹) in cyclic ketenimine **6**. Hence, the probability of depositing energy in vibrational modes above the reaction barrier is higher in **5** than in **6**, which could explain why the broadband IR irradiation tends to promote IR-induced chemistry toward **6**.⁴⁴

Tunneling Calculations

To support the experimental evidence of quantum tunneling effect in the process of formation of ketenimine **6** from cyclic benzazirine **5**, we computed the rate constants without and with tunneling

(using canonical variational transition state theory –CVT– and small curvature tunneling –SCT–, respectively).⁴⁵ The estimated CVT rate constant at 10 K is $1.8 \times 10^{-177} \text{ s}^{-1}$, which indicates that the 5-h to 6-h reaction is impossible to occur. In contrast, the SCT rate constant for the 5-h to 6-h reaction at 10 K (from the ground state at this temperature) is $3.5 \times 10^{-5} \text{ s}^{-1}$ (a half-life time of ~6 hours), which is comparable to experimental result (around 40 times faster). The difference is justifiable considering the difference between the solid matrix experiment and the gas phase computation plus the error of the DFT theoretical method [M06-2X gives an activation energy of $6.2 \text{ kcal mol}^{-1}$, $1.3 \text{ kcal mol}^{-1}$ lower than CCSD(T)]. Thus, the results validate the computational method and at the same time corroborate the observed tunneling effect of the experiments: going from 5 to 6 is a transformation only attainable by a tunneling process from the ground state at cryogenic conditions (see Figure 8). At 20 K the computed SCT rate constant is $3.6 \times 10^{-5} \text{ s}^{-1}$, almost the same as at 10 K, indicating that the first vibrational excited quantum level of the reactant remains practically not thermally populated, and a thermally activated tunneling process should be negligible. This indicates that a marginal increase of the experimental rate at 20 K compared to the 10 K should be attributed to matrix softening.

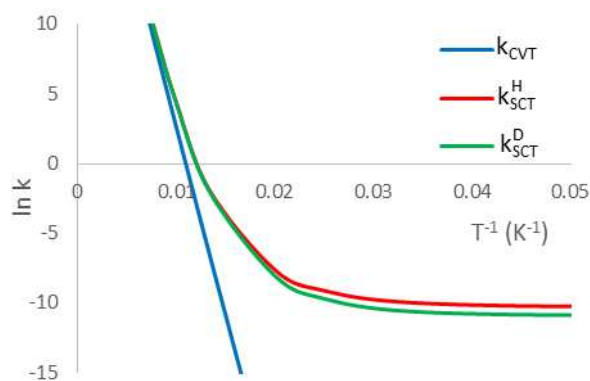
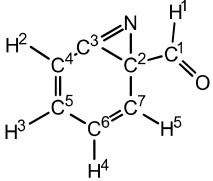


Figure 8. Arrhenius graph for the benzazirine (5-h and 5-d) to cyclic ketenimine (6-h and 6-d) reaction without (CVT) and with (SCT) tunneling correction. Computations indicate that below ~150 K tunneling is the main component of the rate constant, and below 20 K the reaction is completely independent of the temperature (tunneling exclusively from the ground state).

We then proceeded to compute the kinetic isotope effect (KIE) not only for the formyl hydrogen but for all the other atoms as well (using the $^{12}\text{C}/^{13}\text{C}$, $^{14}\text{N}/^{15}\text{N}$, $^{16}\text{O}/^{18}\text{O}$ and H/D mass relations). The results at 10 K are shown in Table 3. As can be seen, **5-d** indeed has a smaller rate of reaction compared to **5-h**, as was observed experimentally. The experimental KIE value was approximately 1.20 ($8.8 \times 10^{-7} \text{ s}^{-1}/7.4 \times 10^{-7} \text{ s}^{-1}$), while theory predicts a KIE of 1.88 (first row in Table 3); this difference can be ascribed to the same reasons explained above, but still both results clearly indicate a significant deceleration of the reaction. Notably, there is a significant negative $\Delta\text{ZPE}^\ddagger$ value of $-0.27 \text{ kJ mol}^{-1}$ in the H/D substitution at the formyl hydrogen which, opposite to the observed KIE, leads to an inverse semi-classical KIE and a potentially faster tunneling due to a lower barrier;⁴⁶ nevertheless, the mass effect of the deuterium substitution strongly overrides this effect. Other H/D substitutions also provide a significant KIE (except for H4). In the case of heavy-atom tunneling, we can see that C3 has the largest KIE, indicating that this is the “tunneling determining atom”, the one with the widest displacement. But most of other atoms also have large KIE, denoting a holistic molecular rearrangement. Interestingly the pivotal nitrogen, with a KIE of only 1.05, is comparatively static and is mostly a “spectator” in the tunneling mechanism. In this sense, the heavy atom tunneling is predominantly carbon tunneling.

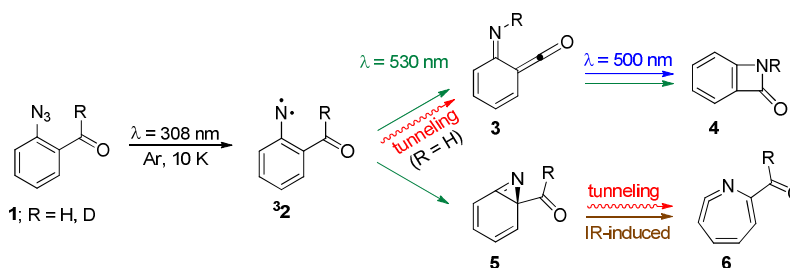
Table 3. Computed kinetic isotope effect for the benzazirine **5** ring expansion for the $^{12}\text{C}/^{13}\text{C}$, $^{14}\text{N}/^{15}\text{N}$, $^{16}\text{O}/^{18}\text{O}$ and H/D isotopic substitutions at 10 K.



Atom	KIE	Atom	KIE
C ¹	1.29	H ¹	1.88
C ²	1.23	H ²	1.80
C ³	1.88	H ³	2.16
C ⁴	1.16	H ⁴	1.05
C ⁵	1.17	H ⁵	1.53
C ⁶	1.04	N	1.05
C ⁷	1.23	O	1.17

CONCLUSIONS

The summary of the experimental results of the photochemistry of protium ³2-h and deuterated ³2-d triplet 2-formyl-phenylnitrene is presented in Scheme 3. Irradiation of ³2, generated in argon matrix at 10 K from 2-formyl-phenylazide **1**, led to the formation of imino-ketene **3** and benzazirine **5**. The imino-ketene **3** was found to subsequently photorearrange to benzoazetinone **4**. The benzazirine **5** was found to undergo spontaneous ring expansion to cyclic ketenimine **6** in the dark at 10 K, despite an estimated reaction barrier of 7.5 kcal mol⁻¹. Moreover, the reaction rate was observed to barely show any increase upon increase of the absolute temperature by a factor of two (from 10 to 20 K). These experimental data clearly provide strong evidence that ring expansion of **5** to **6** occurs by heavy-atom tunneling. Computed rate constants with and without tunneling (SCT and CVT approximation, respectively) confirm that the ring expansion of **5** to **6** can only be attainable by a tunneling process from the ground state at cryogenic conditions. In addition, a small secondary kinetic isotopic effect, corresponding to the deceleration of the reaction upon substitution of protium with deuterium in the formyl group of benzazirine, was predicted theoretically and measured experimentally. Also interesting, it was observed that the ring expansion of **5** to **6** is stimulated by broadband IR radiation. The reaction rate was measured to be more than one order of magnitude faster when the sample at 10 K is exposed to the radiation from the IR light source of FTIR spectrometer.



Scheme 3. Summary of the reactions experimentally observed on the potential energy surface of the aryl nitrene **2**.

Overall, the results unravel a remarkable feature on the potential energy surface of an aryl nitrene. We discovered two isomeric species connected photochemically that both react by quantum tunneling: the 2-formyl-phenylnitrene by proton tunneling, as reported previously,¹⁹ and the corresponding benzazirine by heavy-atom tunneling, as reported here. To the best of your knowledge, this is the first system where interconverted isomers exhibit two different types of tunneling.

EXPERIMENTAL SECTION

Sample: Protium 2-formyl-phenylazide **1-h** and deuterated 2-formyl-phenylazide **1-d** were prepared as described in our previous communication.¹⁹ The deuterium enrichment of sample **1-d** is $\geq 90\%$. Between the experiments, the samples of **1-h** or **1-d** were stored in a glass tube, under vacuum, in refrigerator at +4°C, and in dark. Under such conditions the azides were stable for many weeks

Matrix Isolation IR Spectroscopy: A solid sample of **1-h** or **1-d** was placed in a glass tube that was then connected to a needle valve (SS4 BMRG valve, NUPRO) attached to the vacuum chamber of a helium-cooled cryostat (APD Cryogenics closed-cycle refrigerator with DE-202A expander). Prior to deposition of the matrices, the samples were purified from the volatile impurities by pumping through the cryostat at room temperature. The sample tube with **1-h** or **1-d** was subsequently cooled with an ice-water mixture (at 0°C) to reduce the saturated pressure of the compound and improve the metering function of the needle valve. During the preparation of the matrices, the sample vapors were deposited, together with a large excess of argon (N60, Air Liquide) onto a CsI window at 15 K, used as optical substrate. After the deposition, all samples were cooled down to 10 K and kept at this temperature both during irradiations and during the monitoring of spontaneous decays (unless stated otherwise). The temperature was measured directly at the sample holder window by a silicon diode sensor connected to a digital controller providing stabilization accuracy of 0.1 K.

The mid-IR spectra (4000-400 cm^{-1} range) were recorded using a Thermo Nicolet 6700 Fourier transform infrared spectrometer, equipped with a deuterated triglycine sulphate (DTGS) detector and a

KBr beam splitter, with 0.5 cm^{-1} resolution. To avoid interference from atmospheric H_2O and CO_2 , a stream of dry air was continuously purged through the optical path of the spectrometer. In some experiments, to avoid exposing the sample matrix to the light source of the FTIR spectrometer with wavenumbers higher than 2200 cm^{-1} , the mid-IR spectra were recorded only in the $2200\text{--}400\text{ cm}^{-1}$ range, with a standard Edmund Optics long-pass filter placed between the spectrometer sources and the cryostat.

UV-Vis Irradiation Experiments: The matrices were irradiated, through the outer KBr window of the cryostat, using tunable narrowband ($\sim 0.2\text{ cm}^{-1}$ spectral width) light provided by a signal (visible light) or a frequency-doubled signal (UV range) beam of the Spectra Physics Quanta-Ray MOPO-SL optical parametric oscillator pumped with a pulsed Nd:YAG laser (repetition rate = 10 Hz, duration = 10 ns). The pulse energy for visible and UV-light irradiations was 9-10 mJ and $\sim 1\text{--}3\text{ mJ}$, respectively. Irradiation with UV-light at 308 nm was used to induce the initial photochemistry of the azide precursor (**1-h** and **1-d**) because it matches its first absorption and avoid, as much as possible, the absorption of corresponding product triplet nitrene ($^3\mathbf{2-h}$ and $^3\mathbf{2-d}$) with a maximum at around 326 nm.

Kinetics: Monitoring of the decays of **5-d** into **6-d** and of **5-h** into **6-h** was carried out by successive registrations of infrared spectra, as a function of time. For all of the three different sets of external light ("dark", "filtered IR light", "unfiltered IR light", described above) the infrared spectra were collected using 64 scans. Under such conditions, the collection length of one spectrum equals to 261 seconds. Already during these initial minutes, a part of the photoproduct benzazirine **5** undergoes decay into cyclic ketenimine **6**. In the kinetic analysis, the moment of registration of the first spectrum was assumed to be the origin of decay time, the intensity of the benzazirine **5** bands present in this first spectrum was assumed to be relative 100%, and the amount of cyclic ketenimine **6** present extracted from the same first spectrum (formed between the irradiation and the registration of the first spectrum) was assumed to be relative 0%. The amounts of particular species in the sample were followed by the peak intensities of the most characteristic absorption bands, non-overlapping with absorptions of other species. For this purpose, the following peaks were selected: 1241 cm^{-1} for **5-d** (Table 1), 1890 cm^{-1} for

6-d (Table 2), 1242 cm^{-1} for 5-h (Table S7), 1883 cm^{-1} for 6-h (Table S8). For “unfiltered IR light” kinetics, (Figure 6) the decay of 5-d was monitored for 32 hours and, upon that time, ~20% of the benzazirine remained in the sample. The “dark” decay kinetics of 5-d (Figure 7, left) was monitored for 120 hours and, upon that time, ~75% of benzazirine 5-d still remained in the sample. After that period, the “unfiltered IR light” conditions were implemented, and the decay was followed during subsequent 65 hours (Figure 7, right). During that time, the amount of benzazirine 5-d decreased from ~75% to just ~5%. In a similar experiment with the protium analogue 5-h, ~73% of benzazirine 5-h remained in the sample after 120 hours of applying “dark” conditions. After subsequent 72 hours of observation using the “unfiltered IR light conditions”, the amount of 5-h decreased from ~73% to less than 5%. The amounts of cyclic ketenimine 6 generated in the process of tunneling were then normalized in such a way so that at the end of each monitoring period the sum of 5 and 6 would be 100%. These normalizations assumed a direct quantitative transformation of 5 into 6, which was indeed confirmed spectroscopically. The decays observed in present experiments (presented in Figures 6, 7, S8 and S9) were fitted, for rough estimation of the rate constants, using the equations of a single-exponential decay: $[R]_t = [R]_0 \exp[-k t]$. The rate constants k extracted from these fits, and the corresponding half-lives, are discussed along the text.

Theoretical Calculation: Calculations performed at B3LYP/6-311++G(d,p) level were carried using *Gaussian09*⁴⁷. With the aim of modeling the IR spectra, geometry optimizations at B3LYP/6-311++G(d,p) level were followed by harmonic frequency calculations at the same level. To correct the vibrational anharmonicity, basis set truncation, and the neglected part of electron correlation, the calculated frequencies were scaled by 0.98⁴⁸ (0.97 for the $\nu(\text{N-D})$ mode). The scaled frequencies and the calculated IR intensities were then convoluted with Lorentzian functions having an $\text{fwhm} = 2 \text{ cm}^{-1}$. The integral area of the simulated band equals to the theoretical calculated IR intensity. Due to the broadening, the peak intensities in the simulated spectra are reduced compared with the calculated intensities (in km mol^{-1}), and therefore, are shown in arbitrary units of “relative intensity”. Assignments of vibrational modes were made by inspection of *ChemCraft*⁴⁹ animations.

Tunneling Calculation: Single point energy values were computed at the CCSD(T)-F12/cc-pVTZ-F12//M06-2X/6-311+G(2d,p) level⁵⁰⁻⁵² (coupled cluster computations were carried out with Orca⁵³ version 4.0.1, DFT optimizations with *Gaussian09*⁴⁷). All the computed reaction rates including quantum tunneling were carried out using the multidimensional small curvature tunneling method (SCT)⁵⁴, with step size of 0.001 Bohr, quantized reactant state tunneling (QRST) for the reaction coordinate mode, and at the M06-2X/6-311+G(2d,p) level. Using a multidimensional method to account for “corner-cutting” was critical, as the results using the unidimensional zero-curvature tunneling (ZCT) are three orders of magnitude less for this reaction. All the rates were computed with *Polyrate*⁵⁵, using *Gaussrate*⁵⁶ as the interface with *Gaussian*.

SUPPORTING INFORMATION

The Supporting Information is available free of charge on the ACS Publications website at DOI:

Additional experimental results, IR assignments, and computational data.

AUTHOR INFORMATION

Corresponding Author:

*cmnunes@qui.uc.pt

ORCID

Cláudio M. Nunes: 0000-0002-8511-1230

NOTES

The authors declare no competing financial interest.

ACKNOWLEDGMENT

This work was supported by the Portuguese “Fundação para a Ciência e a Tecnologia” (FCT). The Coimbra Chemistry Centre is supported by the FCT through the project UID/QUI/0313/ 2013, cofunded by COMPETE. C.M.N. and I.R. acknowledge the FCT for Postdoctoral Grant No. SFRH/BPD/86021/2012 and *Investigador FCT* Grant, respectively.

REFERENCES

- (1) *Nitrenes and Nitrenium Ions*; Falvey, D. E.; Gudmundsdóttir, A. D., Eds.; John Wiley & Sons, 2013.
- (2) Gritsan, N.; Platz, M. S. Photochemistry of Azides: The Azide/Nitrene Interface. In *Organic Azides: Syntheses and Applications*; Bräse, S.; Banert, K., Eds.; John Wiley & Sons, 2010; pp. 311–372.
- (3) Platz, M. S. Nitrenes. In *Reactive Intermediate Chemistry*; Moss, R. A.; Platz, M. S.; Jones, M. J., Eds.; John Wiley & Sons, 2004; pp. 501–559.
- (4) Gritsan, N.; Borden, W. T.; Platz, M. The Study of Nitrenes by Theoretical Methods. In *Computational Methods in Photochemistry*; Kutateladze, A. G., Eds.; CRC Press, 2005; pp. 235–356.
- (5) Wentrup, C. *Chem. Rev.* **2017**, *117*, 4562–4623.
- (6) Gritsan, N. P.; Platz, M. S. *Chem. Rev.* **2006**, *106*, 3844–3867.
- (7) Borden, W. T.; Gritsan, N. P.; Hadad, C. M.; Karney, W. L.; Kemnitz, C. R.; Platz, M. S. *Acc. Chem. Res.* **2000**, *33*, 765–771.
- (8) Smith, E.; Collins, I. *Future Med. Chem.* **2015**, *7*, 159–183.
- (9) Tasdelen, M. A.; Yagci, Y. *Angew. Chem. Int. Ed.* **2013**, *52*, 5930–5938.
- (10) Liu, L.; Yan, M. *Acc. Chem. Res.* **2010**, *43*, 1434–1443.
- (11) Bräse, S.; Gil, C.; Knepper, K.; Zimmermann, V. *Angew. Chem. Int. Ed.* **2005**, *44*, 5188–5240.
- (12) Lineberger, W. C.; Borden, W. T. *Phys. Chem. Chem. Phys.* **2011**, *13*, 11792–11813.
- (13) Wijeratne, N. R.; Da Fonte, M.; Ronemus, A.; Wyss, P. J.; Tahmassebi, D.; Wenthold, P. G. *J. Phys. Chem. A* **2009**, *113*, 9467–9473.
- (14) Karney, W.; Borden, W. *J. Am. Chem. Soc.* **1997**, *119*, 1378–1387.
- (15) Inui, H.; Sawada, K.; Oishi, S.; Ushida, K.; McMahon, R. J. *J. Am. Chem. Soc.* **2013**, *135*, 10246–10249.
- (16) Grote, D.; Sander, W. *J. Org. Chem.* **2009**, *74*, 7370–7382.
- (17) Pritchina, E. A.; Gritsan, N. P.; Bally, T. *Phys. Chem. Chem. Phys.* **2006**, *8*, 719–727.
- (18) Morawietz, J.; Sander, W. *J. Org. Chem.* **1996**, *61*, 4351–4354.

- (19) Nunes, C. M.; Knezz, S. N.; Reva, I.; Fausto, R.; McMahon, R. J. *J. Am. Chem. Soc.* **2016**, *138*, 15287–15290.
- (20) Gerbig, D.; Schreiner, P. R. *Angew. Chem. Int. Ed.* **2017**, 9445–9448.
- (21) Ley, D.; Gerbig, D.; Schreiner, P. R. *Org. Biomol. Chem.* **2012**, *10*, 3781–3790.
- (22) Layfield, J. P.; Hammes-Schiffer, S. *Chem. Rev.* **2014**, *114*, 3466–3494.
- (23) Lambert, N.; Chen, Y.-N.; Cheng, Y.-C.; Li, C.-M.; Chen, G.-Y.; Nori, F. *Nat. Phys.* **2012**, *9*, 10–18.
- (24) Borden, W. T. *WIREs Comput. Mol. Sci.* **2015**, *6*, 20–46.
- (25) Two possible additional cases of heavy-atom tunneling are the ring closure reactions of triplet 1,3-diradicals, cyclopentane-1,3-diyl and cyclobutane-1,3-diyl. See refs. 25a and 25b, respectively. Because both reactions require that the triplet 1,3-diradical undergoes ISC to form the singlet product, the rationalization of the mechanism involved is more complex. (25a) Buchwalter, S. L.; Closs, G. L. *J. Am. Chem. Soc.* **1979**, *101*, 4688–4694. (25b) Sponsler, M. B.; Jain, R.; Coms, F. D.; Dougherty, D. A. *J. Am. Chem. Soc.* **1989**, *111*, 2240–2252.
- (26) Orendt, A. M.; Arnold, B. R.; Radziszewski, J. G.; Facelli, J. C.; Malsch, K. D.; Strub, H.; Grant, D. M.; Michl, J. *J. Am. Chem. Soc.* **1988**, *110*, 2648–2650.
- (27) Zuev, P. S.; Sheridan, R. S.; Albu, T. V.; Truhlar, D. G.; Hrovat, D. A.; Borden, W. T. *Science* **2003**, *299*, 867–870.
- (28) Moss, R. A.; Sauers, R. R.; Sheridan, R. S.; Tian, J.; Zuev, P. S. *J. Am. Chem. Soc.* **2004**, *126*, 10196–10197.
- (29) Ertelt, M.; Hrovat, D. A.; Borden, W. T.; Sander, W. *Chem. A Eur. J.* **2014**, *20*, 4713–4720.
- (30) Schleif, T.; Mierez-Perez, J.; Henkel, S.; Ertelt, M.; Borden, W. T.; Sander, W. *Angew. Chem. Int. Ed.* **2017**, *56*, 10746–10749.
- (31) Nandi, A.; Gerbig, D.; Schreiner, P. R.; Borden, W. T.; Kozuch, S. *J. Am. Chem. Soc.* **2017**, *139*, 9097–9099.
- (32) Only the *anti*-form of the deuterated 2-formyl-phenylazide **1-d** precursor, considering the orientation of the –CDO moiety, was populated in the gas phase and deposited in the matrix. Accordingly, only the *anti*-form of nitrene ³**2-d** was generated in the matrix upon photolysis of **1-d**

(see also ref. 19).

(33) In the experimental difference UV-Vis spectrum obtained for triplet nitrene **3**² (ref. 19), the presence of a strong absorption above 350 nm due to imino ketene **3** precluded the identification of weaker absorptions due to the nitrene in this region. However, the occurrence of photochemistry for **3**² with onset at 530 nm is coherent with the estimation of very weak electronic transitions at 449 and 536 nm by TDDFT calculations (ref. 19). Indeed, it has been observed experimentally that triplet arylnitrenes have a characteristic weak feature that extends to 500 nm or higher (ref. 6 and 33a). (33a) Carra, C.; Nussbaum, R.; Bally, T. *ChemPhysChem* **2006**, *7*, 1268–1275.

(34) The conversion of **A** into **B** was also observed during irradiations at 530 nm, but the reaction is much more efficient at 500 nm.

(35) Nunes, C. M.; Reva, I.; Pinho e Melo, T. M. V. D.; Fausto, R. *J. Org. Chem.* **2012**, *77*, 8723–8732.

(36) Dunkin, I. R.; Lynch, M. A.; Withnall, R.; Boulton, A. J.; Henderson, N. *J. Chem. Soc. Chem. Commun.* **1989**, 1777.

(37) Breda, S.; Lapinski, L.; Reva, I.; Fausto, R. *J. Photochem. Photobiol. A Chem.* **2004**, *162*, 139–151.

(38) Tomioka, H.; Ichikawa, N.; Komatsu, K. *J. Am. Chem. Soc.* **1993**, *115*, 8621–8626.

(39) Chapman, O. L.; Le Roux, J.-P. *J. Am. Chem. Soc.* **1978**, *100*, 282.

(40) Dunkin, I. R.; Thomson, P. C. P. *J. Chem. Soc. Chem. Commun.* **1980**, 499–501.

(41) Donnelly, T.; Dunkin, I. R.; Norwood, D. S. D.; Prentice, A.; Shields, C. J.; Thomson, P. C. P. *J. Chem. Soc. Perkin Trans.* **1985**, 307–310.

(42) Bally et al., have developed a protocol of irradiations allowing the selective photoconversion between the three isomeric species in cryogenic matrices: 2,6-difluorophenylnitrene, the corresponding benzazirine and cyclic ketenimine. The approach was based on their different UV-Vis absorption spectra (see ref. 33a): triplet arylnitrenes have a characteristic weak feature that extends to 500 nm or more, benzazirines have a broad feature around 300 nm, and the corresponding cyclic ketenimines have a broad band around 400 nm. Similar protocol was applied by other authors (See refs. 15, 16, 42a, 42b). In the present case, the study of photochemical interconversions between triplet arylnitrene **3**², benzazirine **5**, and cyclic ketenimine **6** might be hampered by an additional photochemical pathway from nitrene **3**² to imino-ketene **3** (which is also photoreactive) and the existence of two tunneling reactions. (42a) Sander, W.; Winkler, M.; Cakir, B.; Grote, D.; Bettinger, H. F. *J. Org. Chem.* **2007**, *72*, 715–724; (42b) Grote, D.; Finke, C.; Neuhaus, P.; Sander, W. *Eur. J. Org. Chem.* **2012**, 3229–3236.

(43) The IR light source (ETC EverGlo) of our FTIR spectrometer, running in normal operating mode,

1 produces radiation essentially only in the 7400 to 50 cm⁻¹ region. This clearly rules out the possibility of
2 the rearrangement of **5** to **6** being promoted by an electronic transition, when the sample is kept under
3 “unfiltered IR light” conditions. Actually, if any radiation capable of inducing electronic excitation
4 reached the sample under “unfiltered IR light” conditions, one would expect the observation of **3** to **4**
5 rearrangement. As described, the rearrangement of **3** to **4** is induced by irradiation at 500 nm, and at this
6 wavelength species **5** does not absorb (TDDFT calculation estimates the first electronic transition of **5** at
7 $\lambda = 332$ nm [$f=0.0093$]).
8
9
10
11
12

13 (44) Examples of isomerization reactions in matrices that consist of two components, tunneling and
14 IR-induced conversion (which may compete), have been previously described. See refs. 30 and 44a-c.

15 (44a) Reva, I.; Nunes, C. M.; Biczysko, M.; Fausto, R. *J. Phys. Chem. A* **2015**, *119*, 2614–2627.

16 (44b) Lapinski, L.; Reva, I.; Rostkowska, H.; Fausto, R.; Nowak, M. J. *J. Phys. Chem. B* **2014**, *118*,
17 2831–2841. (44c) Reva, I.; Nowak, M. J.; Lapinski, L.; Fausto, R. *J. Chem. Phys.* **2012**, *136*, 64511.
18
19
20
21
22

23 (45) Some of us have been working on the predictions of heavy-atom tunneling using SCT
24 computations. For some of the most recent works see refs. 31 and 45a-b. (a) Kozuch, S. *Phys. Chem.*
25 *Chem. Phys.* **2014**, *16*, 7718–7727. (b) Kozuch, S.; Zhang, X.; Hrovat, D. A.; Borden, W. T. *J. Am.*
26 *Chem. Soc.* **2013**, *135*, 17274–17277.
27
28
29

30 (46) Zhang, X.; Datta, A.; Hrovat, D. A.; Borden, W. T. *J. Am. Chem. Soc.* **2009**, *131*, 16002–16003.
31

32 (47) Frisch, M. J.; Trucks, G. W.; Schlegel, H. B.; Scuseria, G. E.; Robb, M. A.; Cheeseman, J. R.;
33 Scalmani, G.; Barone, V.; Mennucci, B.; Petersson, G. A.; Nakatsuji, H.; Caricato, M.; Li, X.;
34 Hratchian, H. P.; Izmaylov, A. F.; Bloino, J.; Zheng, G.; Sonnenberg, J. L.; Hada, M.; Ehara, M.;
35 Toyota, K.; Fukuda, R.; Hasegawa, J.; Ishida, M.; Nakajima, T.; Honda, Y.; Kitao, O.; Nakai, H.;
36 Vreven, T.; Montgomery, Jr., J. A.; Peralta, J. E.; Ogliaro, F.; Bearpark, M.; Heyd, J. J.; Brothers, E.;
37 Kudin, K. N.; Staroverov, V. N.; Keith, T.; Kobayashi, R.; Normand, J.; Raghavachari, K.; Rendell, A.;
38 Burant, J. C.; Iyengar, S. S.; Tomasi, J.; Cossi, M.; Rega, N.; Millam, J. M.; Klene, M.; Knox, J. E.;
39 Cross, J. B.; Bakken, V.; Adamo, C.; Jaramillo, J.; Gomperts, R.; Stratmann, R. E.; Yazyev, O.; Austin,
40 A. J.; Cammi, R.; Pomelli, C.; Ochterski, J. W.; Martin, R. L.; Morokuma, K.; Zakrzewski, V. G.; Voth,
41 G. A.; Salvador, P.; Dannenberg, J. J.; Dapprich, S.; Daniels, A. D.; Farkas, Ö.; Foresman, J. B.; Ortiz,
42 J. V.; Cioslowski, J.; Fox, D. J. *Gaussian 09*, Revision D.01; Gaussian, Inc.: Wallingford, CT, 2013.
43
44
45
46
47
48
49
50
51
52

53 (48) Nunes, C. M.; Reva, I.; Fausto, R.; Begue, D.; Wentrup, C. *Chem. Commun.* **2015**, *51*, 14712–
54 14715.
55

56 (49) Zhurko, G. A. *ChemCraft*, Version 1.8. <http://www.chemcraftprog.com> (2016). Last accessed on
57 November 3, 2017.
58
59
60

- (50) Ten-no, S.; Noga, J. *WIREs Comput. Mol. Sci.* **2012**, 2, 114–125.
- (51) Zhao, Y.; Truhlar, D. G. *Theor. Chem. Acc.* **2008**, 120, 215–241.
- (52) Peterson, K. A.; Adler, T. B.; Werner, H. J. *J. Chem. Phys.* **2008**, 128, 84102.
- (53) Neese, F. *WIREs Comput. Mol. Sci.* **2012**, 2, 73–78.
- (54) Fernandez-Ramos, A.; Ellingson, B. A.; Garrett, B. C.; Truhlar, D. G. In *Rev. Comput. Chem.*; Lipkowitz, K. B., Cundari, T. R., Eds.; John Wiley & Sons, 2007; Vol. 3, pp 125–232.
- (55) Zheng, J.; Bao, J. L.; Meana-Pañeda, R.; Zhang, S.; Lynch, B. J.; Corchado, J. C.; Chuang, Y.-Y.; Fast, P. L.; Hu, W.-P.; Liu, Y.-P.; Lynch, G. C.; Nguyen, K. A.; Jackels, C. F.; Fernandez Ramos, A.; Ellingson, B. A.; Melissas, V. S.; Villà, J.; Rossi, I.; Coitiño, E. L.; Pu, J.; Albu, T. V.; Ratkiewicz, A.; Steckler, R.; Garrett, B. C.; Isaacson, A. D.; Truhlar, D. G. *Polylrate*—version 2016-2A, University of Minnesota, Minneapolis, 2016.
- (56) Zheng, J.; Zhang, S.; Corchado, J. C.; Meana-Pañeda; Chuang, Y.-Y.; Coitiño, E. L.; Ellingson, B. A.; Truhlar, D. G.; *Gaussrate* 2016, Department of Chemistry and Supercomputing Institute, University of Minnesota, Minneapolis, Minnesota 55455.

Graphical TOC image

